



Thermosensitive Cu₂O-PNIPAM core-shell nanoreactors with tunable photocatalytic activity

Received 00th January 20xx,
Accepted 00th January 20xx

DOI: 10.1039/x0xx00000x

www.rsc.org/

He Jia,¹ Rafael Roa,¹ Stefano Angioletti-Uberti,^{1,2} Katja Henzler,³ Andreas Ott,¹ Xianzhong Lin,⁴ Jannik Möser,⁵ Zdravko Kochovski, Alexander Schnegg,⁵ Joachim Dzubiella,^{1,2} Matthias Ballauff,^{1,2} Yan Lu^{1*}

We report a facile and novel method for the fabrication of Cu₂O@PNIPAM core-shell nanoreactors using Cu₂O nanocubes as the core. The PNIPAM shell not only effectively protects the Cu₂O nanocubes from oxidation, but also improves the colloidal stability of the system. The Cu₂O@PNIPAM core-shell microgels can work efficiently as photocatalyst for the decomposition of methyl orange under visible light. A significant enhancement in the catalytic activity has been observed for the core-shell microgels compared with the pure Cu₂O nanocubes. Most importantly, the photocatalytic activity of the Cu₂O nanocubes can be further tuned by the thermosensitive PNIPAM shell, as rationalized by our recent theory.

INTRODUCTION

Cu₂O is a well-known p-type semiconductor with direct band gap of 2.17 eV. It has a great potential for a wide range of applications, e.g. in solar energy conversion, lithium-ion batteries, gas sensors, photocatalytic degradation of dye molecules, propylene oxidation and photoactivated water splitting. The properties of the Cu₂O nanoparticles are strongly dependent on their shape. Hence, there is a growing interest in the synthesis of Cu₂O nanostructures with defined shape.^{1–6} Thus, Cu₂O nanocubes, octahedral, nanocages, spheres, nanowires and other highly symmetrical structures have already been reported.^{7,8}

A main drawback for further applications of Cu₂O nanoparticles is that Cu₂O is easily oxidized in water and the nanostructure of Cu₂O can be destroyed depending on external conditions such as pH or visible light. For this reason, a simple and effective method providing protection of Cu₂O-based nanostructures from oxidation is highly desirable. Parecchino et al. successfully improved the chemical stability of a Cu₂O layer in water through atomic layer deposition of multiple protective layers of Al-doped zinc and titanium oxide.^{9,10} Wang's group reported that both CuO and carbon can be used to protect Cu₂O films and nanofibers.^{11,12} Notably,

the aforementioned protection strategies have all been applied to extended one- and two-dimensional phases. However, little has been reported in the literature regarding the effective protection of Cu₂O nanoparticles. In this regard, Yang et al.¹³ and Su et al.¹⁴ have successfully synthesized Cu₂O@SiO₂ core-shell nanoparticles, but unfortunately the SiO₂ shell makes them aggregate more easily, preventing further study on their surface properties.

Recently, shells of poly(*N*-isopropylacrylamide) (PNIPAM) core-shell microgels have been used to modify inorganic nanoparticles.^{15,16} In this way, the nanoparticles encapsulated inside PNIPAM shells can be prevented from aggregation in aqueous solution.¹⁷ For example, Zhao¹⁸ and co-workers reported the fabrication of gold nanoparticles with a thin PNIPAM shell, proposed as a drug delivery system. Of great relevance for catalytic applications is also the fact that the catalytic properties of the embedded nanoparticles can be tuned by the swelling and deswelling of the PNIPAM microgels.^{19–22} In this regard, Liz-Marzán et al.²³ developed different kinds of core-shell hybrid systems via growth of PNIPAM gels on the surface of metal nanoparticles. Recently, some of us presented a theory for the diffusion- and solvation-controlled contribution to the reaction rate of such a “nanoreactor”.²⁴ There, it was demonstrated that the thermosensitive shell can be used to enhance or reduce the local concentration and permeability of a given reactant and thus increase or decrease the total catalytic activity of the embedded nanoparticle, respectively. Thus, core-shell systems consisting of a catalytically active nanoparticle and a polymeric shell present a novel type of nanoscopic catalyst with tunable properties.

To the best of our knowledge, until now no work has been reported on the colloidal stable Cu₂O nanoparticles modified

¹Soft Matter and Functional Materials, Helmholtz-Zentrum Berlin für Materialien und Energie, Hahn-Meitner-Platz 1, Berlin (Germany)

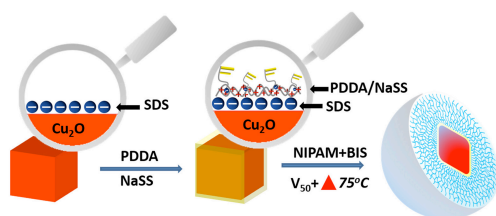
²Institut für Physik, Humboldt-Universität zu Berlin, Newtonstr. 15, Berlin (Germany)

³Paul Scherrer Institut, 5232 Villigen PSI (Switzerland)

⁴Heterogeneous Materialien und Energie, Helmholtz-Zentrum Berlin für Materialien und Energie, Hahn-Meitner-Platz 1, Berlin (Germany)

⁵Institute for Nanospectroscopy Helmholtz-Zentrum Berlin für Materialien und Energie, Kekulestr 5, Berlin (Germany).

with PNIPAM shells. Such functional hybrid nanoparticles will not only improve the stability of sensitive semiconductor nanoparticles, but also be applied as “nanoreactors” with stimuli-responsibility. Here we present for the first time the synthesis and characterization of $\text{Cu}_2\text{O}@$ PNIPAM core-shell hybrid nanoparticles using cubic-shaped Cu_2O nanoparticles as core. Scheme 1 shows the procedure of the main synthesis step for this system, i.e. coating of the nanoparticle with the PNIPAM shell: Without modification with a SiO_2 or polystyrene interlayer²⁵⁻²⁷, a single Cu_2O nanocubes is encapsulated in a thermosensitive PNIPAM shell which prevents the aggregation. The synthesis proceeds in two steps: Firstly, the surface of the Cu_2O -cubes is modified by an interlayer of poly(diallyldimethylammonium chloride) (PDDA) and sodium styrene sulfonic acid (NaSS). In the second step, the PNIPAM-shell is attached to the cubes by a precipitation polymerization. We demonstrate that the photocatalytic activity of the Cu_2O nanocubes can be significantly enhanced by the PNIPAM shell, which can be further tuned by temperature mediated by the thermosensitive shell as suggested by theory.²⁴ The present work opens a new way for the surface modification of Cu_2O nanocubes, which will have a great potential for the applications of Cu_2O nanoparticles. In addition, such core-shell “nanoreactor” system is essential to understand the effect of PNIPAM shell on properties of metal or metal oxide nanomaterials.



Scheme 1. Schematic illustration of the procedure used to coat PNIPAM on the surface of Cu_2O nanocubes. With sodium dodecyl sulfate (SDS) as the surfactant, the surfaces of Cu_2O nanocubes are negatively charged. By charge interaction, NaSS was modified on the surface of Cu_2O nanocubes using PDDA as a medium. Under high temperature, polymerization is initiated by the positive initiator V50 and PNIPAM-shell is coated around Cu_2O nanocubes.

Experimental Section

MATERIALS AND METHODS

Materials: Copper chloride (CuCl_2), sodium dodecyl sulfate (SDS), sodium hydroxide (NaOH), sodium ascorbate, poly(diallyldimethylammonium chloride) (20 wt.% in H_2O) (PDDA), 4-styrenesulfonic acid sodium salt hydrate (NaSS), methyl orange (MO), 5,5-dimethyl-pyrroline N-oxide (DMPO), N-isopropylacrylamide (NIPAM) and N,N'-methylene-bis-acrylamide (BIS) were supplied by Aldrich. 2,2'-azobis(2-

methylpropionamide dihydrochloride) (V50) was supplied by Fluka. All of the reactants were used without further purification. Water was purified by a Milli-Q system.

Synthesis of Cu_2O nanocubes: Cu_2O nanocubes with size of 259 ± 19 nm were synthesized by seed-mediated reaction modified with the method reported by Michael H. Huang's group.²⁸ Briefly, at first, a volume of 10 mL aqueous solution containing 10^{-3} M CuCl_2 and 3.3×10^{-2} M sodium dodecyl sulfate (SDS) was prepared. Then 250 μL of 0.2 M sodium ascorbate and 500 μL of 1 M NaOH solution was added sequentially with shaking for 5 s to prepare the seeds solution. 1 mL of this seeds solution was transferred to 9 mL solution containing 10^{-3} M CuCl_2 and 3.3×10^{-2} M SDS with shaking for 10 s as the seeds solution for the next step. The same process was repeated for three times. In the last step, the volume of the reaction solution was scaled up to 81 mL. 9 mL seeds solution from the previous step was transferred into it. After shaking for 15 s, 2.25 mL of 0.2 M sodium ascorbate and 4.5 mL of 1M NaOH was added separately with shaking for 8 s. After standing at room temperature in a dark place for 2 h, the color of the solution became orange due to the formation of Cu_2O nanocubes. Then, the Cu_2O nanocubes were washed by centrifugation with the speed at 3500 rpm in water for 20 min and dispersed into 10 mL H_2O .

Synthesis of $\text{Cu}_2\text{O}@$ PNIPAM core-shell nanoparticles: In the first step, Cu_2O nanocubes were modified with PDDA and NaSS as the follows. 2.6 g PDDA was diluted with 27.5 mL H_2O and then 10 mL NaSS (0.024 M) solution was added with the rate of 20 mL/h. After stirring for another 2 hours at a speed of 500 rpm, 10 mL Cu_2O nanocubes solution was added into the mixed solution slowly. The excess PDDA and NaSS were removed by centrifugation (3500 rpm, 15 min) and the modified Cu_2O nanocubes were dispersed into 5 mL H_2O . The $\text{Cu}_2\text{O}@$ PNIPAM core-shell nanoparticle was prepared by precipitation polymerization. Under continuous vigorous stirring and nitrogen atmosphere, the solution containing the modified Cu_2O nanocubes was heated to 75 °C. Thereafter, 1 mL V50 (0.018M) solution was added drop by drop as the initiator. The polymerization was started immediately with the addition of 29 mg NIPAM and 5.1 mg BIS (dissolved in 1 mL H_2O). The orange solution became turbid after 10 min and the reaction was run for 2 h. The composite particles were then purified by centrifugation and redispersion in water several times.

CHARACTERIZATION

The hydrodynamic radius of the samples as a function of temperature was conducted by Zetasizer (Malvern Zetasizer Nano ZS ZEN 3500). The UV-vis spectra were measured by a Lambda 650 spectrometer supplied by Perkin-Elmer or Agilent 8453 with a temperature controlled sample holder with an accuracy of ± 0.1 °C. Transmission electron microscope (TEM) images were done with JEOL JEM-2100 at 200kV. XRD measurements were performed in a Bruker D8 diffractometer in the locked coupled mode (scanning angle from 10° to 90°) with Cu K α 1 radiation, the incident wavelength is 1.5406 Å. For the accomplished measurements the acceleration voltage is set to 40 kV and the filament current to 40 mA. The amount of

Cu₂O in the Cu₂O@PNIPAM core-shell nanoparticles was determined by thermogravimetric analysis (TGA) using a Netsch STA 409PC LUX. Fifteen milligrams of dried sample was heated to 800 °C under a constant argon flow (30 mL/min) with a heating rate of 10 K/min. Scanning electron microscope (SEM) measurements were done in a SEM LEO GEMINI 1530. The size and size distribution of Cu₂O nanoparticles were measured using Image J software based on their TEM images. At least 100 units were counted.

Photocatalytic measurements: For testing the photocatalytic activity, 10 mL Cu₂O@PNIPAM nanoparticles (0.10 wt. %) were dispersed into 90 mL of an aqueous solution containing 15.6 mg/L methyl orange. The samples were first stirred in the dark for 30 min in order to ensure the adsorption of MO into the Cu₂O@PNIPAM core-shell nanoparticles. A 500 W xenon lamp was used as the light source, which was placed 20 cm away from the samples. UV-vis absorption spectra of the samples were taken every 30 min by removing the cap to withdraw the solution. The temperature of the reaction was controlled by a water bath with an accuracy of $\pm 0.2^\circ\text{C}$. The reaction rate k can be defined through normalization of k_{app} to the total surface of the Cu₂O nanocubes in the system. TGA (see Fig. S8) and TEM results have been used to obtain the amount and size of Cu₂O nanocubes in the core-shell nanoparticles. For the calculation of the surface area (S) of the Cu₂O nanocubes in the core-shell nanoparticles, the density of Cu₂O (6.00 g cm⁻³) was used.

Cryogenic transmission electron microscopy: Cryo-TEM specimens were vitrified by plunging the samples into liquid ethane using an automated plunge freezer (Vitrobot Mark IV, FEI). The lacey carbon copper grids (200 mesh, Science Services) have been pretreated by 10 seconds of glow discharge and equilibrated for 5 minutes at 15 °C or 50 °C inside the plunge freezer. Approximately 5 μL of a pre-temperated 0.025 wt. % solution were given on the TEM grids and equilibrated at the adjusted temperature for 2 minutes in a water-saturated atmosphere. After blotting the liquid the specimen were vitrified, inserted into a pre-cooled Gatan 914 sample holder and transferred into a JEOL JEM-2100, operating at 200kV.

Near edge X-ray absorption fine structure – transmission X-ray microscopy (NEXAFS-TXM): Sample preparation for NEXAFS-TXM: ²⁹ The carbon coated copper grids have been pretreated by 10 s of glow discharge. Approximately 5 μL of a 0.1 wt% dispersion of the particles was deposited on a TEM copper grid with a carbon support film (200 meshes, Science Services, Munich, Germany). The grids were dried at room temperature. The NEXAFS-TXM spectra were recorded on the O-K-edge and the Cu-L_{2,3}-edge with the HZB-TXM which is installed at the undulator beamline U41-FSGM at the electron storage ring BESSY II, Berlin, Germany. It provides a high spatial resolution close to 10 nm (half-pitch) and a spectral resolution up to $E/\Delta E \approx 10^4$. Typical spectra are presented for each set of measurements. The TXM allows measurements to be taken at room or liquid nitrogen temperature in a vacuum of 1.3×10^{-9} bar. The spectra were recorded at room temperature in transmission mode by taking a sequence of images over a range of photon energies covering the investigated absorption

edges with a calculated $E/\Delta E > 5800$ for the Cu-L_{2,3}-edge and $E/\Delta E > 12000$ for the O-K-edge. Note that the exit slit of the monochromator was set to 9 μm for the Cu-L_{2,3}-edge and 7 μm for the O-K-edge resulting in the given calculated monochromaticity values. The exposure time for one image with 1340×1300 pixels was 40 s for the Cu-L_{2,3}-edge and 4 s for the O-K-edge to achieve a sufficient signal to noise ratio in the images. Taking an image stack with up to 226 images at different energies needs inherently about 45 to 120 min because of all necessary movements, exposure time, and camera read out time and image storage. The NEXAFS spectra were normalized since the photon flux varies as a function of photon energy ($h\nu$) and time in the object field (x, y). The normalization was performed by dividing the intensity $I(x, y, h\nu)$ recorded on a single nanostructure by the intensity $I_0(x+\Delta x, y+\Delta y, h\nu)$ recorded in its sample free proximity at position ($x+\Delta x, y+\Delta y$). Both $I(x, y, h\nu)$ and $I_0(x, y, h\nu)$ were recorded within the same image stack since bare regions in the vicinity of the nanostructures permit the measurement of I_0 .

Electron spin resonance (ESR): Continuous wave ESR (cwESR) spectra were obtained on a Bruker ESP 300 spectrometer with a Bruker ER-4122 super high quality factor (SHQ) resonator at room temperature. During the ESR measurements samples immersed in the ESR resonator were illuminated through a 250 W cold halogen lamp (Schott KL 2500 LCD). For spin trapping 5,5-dimethyl-pyrroline N-oxide (DMPO) was used. A 50 μL aqueous solution of 50 mg/mL DMPO was mixed with 50 μL of Cu₂O nanoparticle solution with a concentration of 0.20 mg/mL for the Cu₂O@PNIPAM core-shell microgels and 0.15 mg/mL for the pure Cu₂O nanocubes, respectively, in order to ensure an equal amount of Cu₂O in both samples. 20 μL of the mixed sample solution was filled into a Q-band ESR sample tube (inner diameter 1 mm). The resonator was critically coupled yielding quality factors of 4000-5000. Magnetic field modulation for phase-sensitive detection by means of a lock-in amplifier was employed at a frequency of 100 kHz and a peak-to-peak amplitude of 1 G. An incident microwave power of 2 mW was used for all measurements. Spectra were normalized by resonator quality and sample volume. The main text of the article should appear here with headings as appropriate.

RESULTS AND DISCUSSION

Prior to this coating step, Cu₂O nanocubes were initially prepared by seed-mediated method using sodium dodecyl sulfate (SDS) as the capping surfactant.²⁸ As shown in Figure 1a, Cu₂O nanocubes with size of 259 ± 19 nm were synthesized. As the interlayer, PDDA with NaSS was adsorbed due to the charge attraction. The ratio of positive and negative charges contained in PDDA and NaSS is 1:0.074. Thus, after mixing with NaSS, there are still large amounts of positive charges in PDDA chains. PDDA/NaSS is firmly attached to the negatively-charged surface of the SDS stabilized cubes as can be seen from the surface zeta potential which changed from -21.2 mV to 53 mV. The double bonds supplied by the NaSS attached to the surface help the chemical bonding of the PNIPAM shell on the Cu₂O core surface via a precipitation

polymerization. Without this surface modification, most of the Cu_2O nanocubes aggregate quickly.

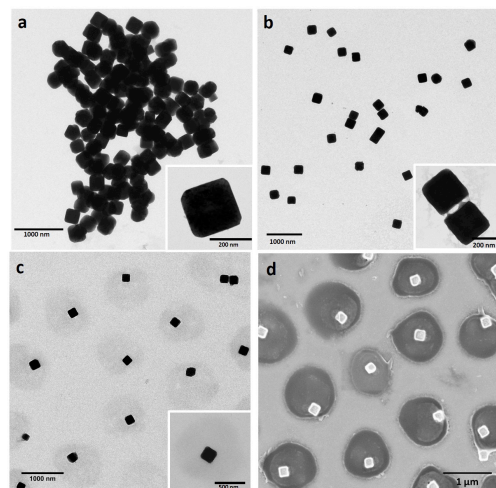


Figure 1. TEM images of (a) Cu_2O nanocubes, (b) Cu_2O @PDDA-NaSS, (c) Cu_2O @PNIPAM core-shell nanoparticles; (d) SEM image of Cu_2O @PNIPAM core-shell nanoparticles.

As shown in Figure 1b, well-dispersed Cu_2O nanocubes were obtained after PDDA/NaSS coating, which was due to the large number of positive charges provided by PDDA. From the inset TEM image in Figure 1b, a very thin PDDA/NaSS layer can be observed clearly. The successful coating of PNIPAM shell on the Cu_2O nanocubes surface was first confirmed by TEM and SEM images as shown in Figure 1c and 1d. The PNIPAM shell was uniformly wrapped around the surface of Cu_2O nanocubes and all of the Cu_2O nanoparticles retained their cubic shapes. Since PNIPAM promotes strong hydrophilic repulsion below the lower critical solution temperature (LCST)³⁰⁻³⁵, the Cu_2O @PNIPAM core-shell nanoparticles are well separated from each other, which can be seen clearly from the overview TEM image of Cu_2O @PNIPAM in Figure 2a. Figure 2b shows a cryo-TEM image of the particles prepared at room temperature. The thickness of the PNIPAM shell was about 360 nm, which agreed well with the thickness of the PNIPAM shell determined by DLS at room temperature in water (marked as a dashed line in Figure 2b).

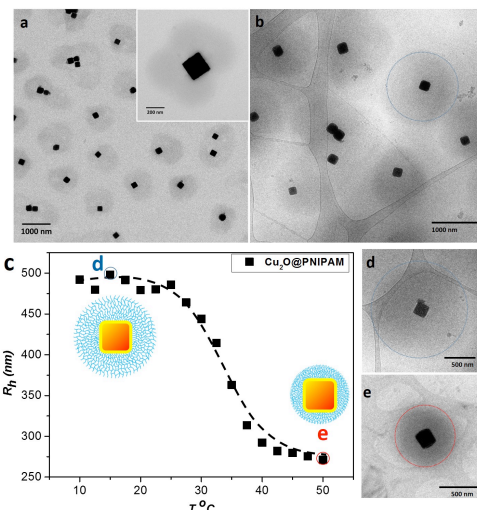


Figure 2. (a) Overview TEM image of Cu_2O @PNIPAM core-shell nanoparticles, (b) Cryo-TEM image of Cu_2O @PNIPAM core-shell nanoparticles (Dashed circle indicate the size of the PNIPAM shell in swollen state at room temperature determined by DLS), (c) Hydrodynamic radius of Cu_2O @PNIPAM core-shell nanoparticles as a function of temperature in aqueous solution, (d,e) Cryo-TEM images of Cu_2O @PNIPAM core-shell nanoparticles in swollen state at 15 °C and in shrunken state at 50 °C, respectively.

DLS measurements of Cu_2O @PNIPAM core-shell nanoparticles shown in Figure 2c proved the thermosensitivity of PNIPAM shell as expected. A well-defined volume phase transition is observed around 32 °C for the Cu_2O @PNIPAM core-shell system. Figure 2d and Figure 2e show the cryo-TEM images of the core-shell nanoparticles at 15 °C and 50 °C, which are in perfect agreement with the DLS data (see point d and point e on the DLS curve Fig. 2c). Below the LCST, the PNIPAM shell is fully swollen in the water solution (see Figure 2d and Figure 2e). When the temperature is increased to 50 °C, the water in the PNIPAM network is extruded, leading to the shrinkage of the PNIPAM shell (see Figure 2d and Figure 2e).

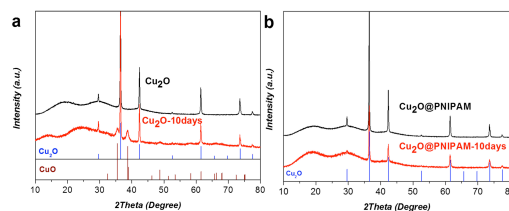


Figure 3. XRD patterns of (a) Cu_2O nanocubes without coating PNIPAM: kept in water at room temperature for 10 days (red)

and fresh prepared (black). (b) $\text{Cu}_2\text{O}@$ PNIPAM core-shell nanoparticles: kept in water at room temperature for 10 days (red) and fresh prepared (black). As reference, standard XRD patterns of CuO (JCPDS: No.45-0937) and Cu_2O (JCPDS: No.65-3288) are shown in the Figures.

The resulted $\text{Cu}_2\text{O}@$ PNIPAM core-shell nanoparticles present a much more colloidal stable system than the pure Cu_2O nanocubes. As shown in Figure s2 in the supporting information, the core-shell nanocubes were still stable in water after standing overnight at room temperature. On the contrast, without PNIPAM coating, all of the Cu_2O nanocubes precipitated at the bottom after the same treatment.

The XRD patterns of Cu_2O nanocubes without PNIPAM shell are presented in Figure 3a. The peaks at $2\theta = 29.63^\circ$, 36.50° , 42.40° , 52.58° , 61.52° , 73.70° and 77.57° correspond to the Bragg reflections of Cu_2O nanocrystals indicating the production of fresh Cu_2O . After storing in water in a dark place for 10 days, new peaks at $2\theta = 35.5^\circ$, 38.34° , 38.66° and 48.8° corresponding to the Bragg reflections of CuO are observed. This indicates the cubic structure of the Cu_2O has been destroyed due to the formation of CuO . Meanwhile, the color of the solution changed from orange to dark green as shown in Figure s3a in the supporting information. Compared with the freshly prepared Cu_2O nanocubes, PNIPAM-modified nanocubes also preserve all of the characteristic Cu_2O peaks, and no other peaks were found, indicating that none of the Cu_2O in these particles was oxidized during the process of coating with PNIPAM (as shown in Figure 3b). In addition, after storing for 10 days under the same condition used with pure Cu_2O nanocubes, no $\text{Cu}_2\text{O}@$ PNIPAM core-shell nanoparticles were oxidized to CuO , as proved by the XRD patterns in Figure 3b. Moreover, all of the Cu_2O maintained the cubic structure and no aggregation was observed in the system (see Figure s3b). Obviously, the PNIPAM-shell is capable of preventing the oxidation of Cu_2O in an efficient manner.

A further proof of the protection by the PNIPAM shell can be given by NEXAFS measurement for the $\text{Cu}_2\text{O}@$ PNIPAM core-shell nanoparticles, which have been kept in water at room temperature for 100 days. Near edge X-ray absorption fine structure spectroscopy (NEXAFS) in combination with transmission X-ray microscopy (TXM) has been used to test the samples for the existence of Cu^{2+} at crystal defect sites or amorphous CuO . The NEXAFS spectroscopy provides chemical sensitivity and the TXM gives the possibility to the analysis of single particles.

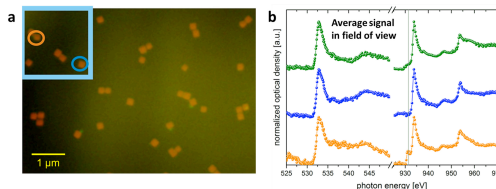


Figure 4. (a) TXM micrograph of the Cu_2O -nanocubes@PNIPAM at two different photon energies: The red channel depicts the nanocubes with Cu_2O , and the green channel refers to CuO . (b) NEXAFS-spectra of the average signals over all $\text{Cu}_2\text{O}@$ PNIPAM core-shell nanoparticles in field of view (green line) and the marked particles in the inset of micrograph on the left hand side at the O-K-edge and the Cu-L_{2,3}-edge (blue and orange lines)

Figure 4a shows a NEXAFS-TXM micrograph in false color representation. The red channel is sensitive to Cu_2O whereas the green channel is sensitive to CuO . The contrast of the PNIPAM shell is too low to be resolved. Figure 4a demonstrates that almost all particles consist of copper(I)-oxide. Only very few small green points on the surface of the Cu_2O nanocubes can be found in Figure 4a, which leads to the small shoulder around 930.8 eV in the spectrum of orange marked particle as shown in Figure 4b. A similar shoulder can be also found in the spectra of freshly synthesized Cu_2O nanoparticles (Figure s4). Thus, this signal is most probably related to side products from the synthesis of the Cu_2O nanocubes, which could not be removed during the purification step or from the preparation process for the TXM measurement. In addition, for both $\text{Cu}_2\text{O}@$ PNIPAM core-shell nanoparticles and the bare Cu_2O nanocubes, this shoulder became much smaller in the spectrum of the average signals over all particles in field of view stating the extremely low proportion of Cu^{2+} in the systems. The NEXAFS-TXM results indicate that the PNIPAM shell can protect effectively the Cu_2O nanocubes from oxidation for at least months.

Figure s9 shows TEM images of individual Cu_2O nanocubes before and after PNIPAM coating and their corresponding selected area electron diffraction (SAED) patterns. The TEM images are provided to show the exact orientations of the Cu_2O nanocubes for the SAED patterns. The circular field of view results from the SA aperture that was inserted to show the actual regions of the sample contributing to the diffraction patterns. These were indexed by comparing with simulated {100} Cu_2O single crystal diffraction patterns using CrystalMaker and SingleCrystal (CrystalMaker Software Ltd, Oxfordshire, UK). The SAED patterns shown in Figure s9 a2 and b2 directly demonstrate that after the modification with PNIPAM, the nanocubes are still Cu_2O without oxidation, since the spacings are not consistent with the monoclinic structure of CuO . The PNIPAM coating doesn't create additional diffractions spot due to its amorphous structure.

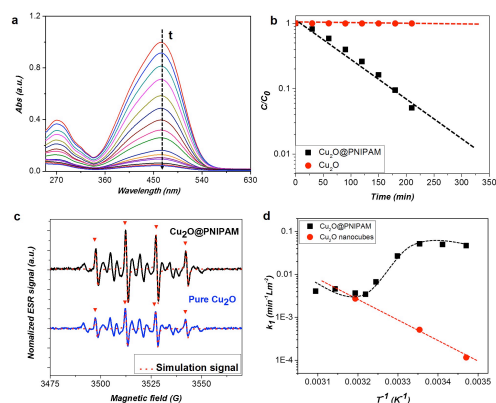


Figure 5. (a) UV-vis absorption spectra of MO as a function of irradiation time using Cu₂O@PNIPAM core-shell nanoparticles as the photocatalyst. (b) Kinetic analysis of MO reduced by Cu₂O@PNIPAM core-shell nanoparticles and pure Cu₂O nanocubes at room temperature (c) ESR spectra of aqueous dispersions of Cu₂O@PNIPAM core-shell nanoparticles (upper red trace) and pure Cu₂O nanocubes (lower black trace) with DMPO spin traps added. Triangles indicate the four ESR lines characteristic DMPO-•OH radicals. The overlaid traces are simulations of the DMPO-•OH signal using the MATLAB library EasySpin. (d) The reaction rate k_1 (rate constant k_{app} normalized to the surface area of Cu₂O nanocubes) at different temperatures for the bare Cu₂O nanocubes (circles) and the Cu₂O@PNIPAM core-shell nanoreactors system (squares).

The photocatalytic activity of Cu₂O@PNIPAM core-shell nanoparticles has been determined by monitoring the photodegradation of methyl orange (MO) under visible light. Here the decay of the strong adsorption at 464 nm is measured as a function of time (Figure 5a; see also Fig. S5). The pure Cu₂O nanocubes are not photocatalytically active at 15°C as shown in Figure 5b.⁸ To compare the photocatalytic activity of different systems directly, the reaction rate k , i.e. the experimentally measured reaction rate normalized to the total surface of the Cu₂O nanocubes, has been applied. As we previously showed, this normalized quantity can be directly linked to the catalytic properties of a single particle.²⁴ It is found that the reaction rate is extremely small for the pure Cu₂O nanocubes at 15°C as expected ($k_{Cu_2O-15^\circ C} = 1.16 \times 10^{-4} \text{ Lmin}^{-1}\text{m}^{-2}$). Cu₂O nanocubes contain mostly {100} facets which have 100% saturated oxygen bonds. These {100} facets are neutral and there is no strong driving force for the adsorption of the negatively charged dye molecules onto the surface of the cubic Cu₂O nanocrystals.^{7,36} Thus, the low reaction rate observed here is in accordance with similar observations of literature.^{7,37,38}

Instead, after modification by a PNIPAM shell, the photocatalytic activity of Cu₂O nanocubes was significantly enhanced ($k_{Cu_2O@P-15^\circ C} = 4.67 \times 10^{-2} \text{ Lmin}^{-1}\text{m}^{-2}$). Figure 5b displays the temporal decay of MO as the function of time for the

Cu₂O@PNIPAM core-shell nanoparticles and the pure Cu₂O nanocubes at 15°C. After irradiation for 4 h, the fraction of remaining amount of MO was ca. 3% in the presence of the Cu₂O@PNIPAM core-shell nanoparticles, compared to 99.4% in the case of pure Cu₂O nanoparticles.

The significantly enhanced photocatalytic efficiency of Cu₂O@PNIPAM core-shell systems over the bare nanoparticles has the following reasons: Firstly, the colloidal stability of Cu₂O@PNIPAM is much higher than that of pure Cu₂O nanocubes and no aggregation is seen for the core-shell Cu₂O@PNIPAM particles during the photocatalytic reaction, thus leading to a larger effective catalytic area for the reaction to occur.

Furthermore, absorption data of reactants to the nanoreactors (see supporting information) also indicate a high binding affinity of the hydrogel shell with average reactant concentrations two orders of magnitude higher in the shell than in the bulk. Zeta potential measurements for the core-shell systems, showing a decrease of +13.7 mV to -5.3 mV upon adding the negatively charged MO to the suspension, support the picture of MO enrichment in the shell. This result indicates that also a higher local concentration of MO adjacent to the nanoparticle may be achieved. As we find that the reaction is fully surface-controlled (i.e., the reactant diffusive transport is much faster than the surface reaction, see supporting information), MO enrichment at the nanocube would lead proportionally to a higher surface rate.²⁴ However, details on such a rate enhancement depend on the exact spatial partitioning of the MO molecules in the nanoreactor what is experimentally not easily accessible.

Another reason is related to the stronger absorption of light and narrower band gap in case of the core-shell particles (see Fig. S6).³⁹⁻⁴¹ This in turn leads to a higher concentration of hydroxyl radicals which are the active species in the process of photodegradation of MO right at the nanocube.^{42,43} As our reaction is fully surface-controlled, the total rate is directly proportional to the local concentration of the hydroxyl radicals and thus increases.

In detail, ESR spin trapping with DMPO was employed⁴⁴ to detect the concentration of hydroxyl radicals in illuminated solutions for pure Cu₂O nanocubes as well as for Cu₂O@PNIPAM core-shell nanoparticles. Both traces in Figure 5d contain a large variety of ESR resonances. Among them 4 peaks with relative intensities of 1:2:2:1 at $g=2.0054$ with a hyperfine splitting of $a_N=a_{H\beta}=15.0 \text{ G}$ can be clearly assigned to the DMPO-•OH adducts. The assignment was confirmed by a simulation of the DMPO-•OH signal by means of the MATLAB simulation toolbox EasySpin⁴⁵ (see Figure 5d). These lines are present in both solutions upon illumination. For the Cu₂O@PNIPAM core-shell nanoparticles the DMPO-•OH signal is at least two times stronger as compared to pure Cu₂O nanocubes. This indicates that much more •OH have been effectively generated by Cu₂O@PNIPAM core-shell microgels than by pure Cu₂O nanocubes.

The influence of temperature on the photocatalytic activity has been studied as well. As shown in Figure 5d, compared to the rate constant of bare Cu₂O nanocubes at different

Joachim Dzubiella 19/2/2018 10:42

Comment [1]: Of course, stability is an issue but shouldn't we comment at least a little on the possible effects chemical changes? Before that paragraph, we discuss lengthily all the changes that occur upon the chemical modifications, i.e., coating with SDS, PDSA, NaSS, PNIPAM, but we do not mention much about its effects on the surface rate (only the different production of OH radicals.) While the intrinsic surface reaction may also change a lot, we do not mention anything about it. Of course, we do not know how much it changes, but shouldn't we honestly discuss the possibility that it may change and perhaps in part accounts for the changes in the rate? Or did I misunderstand something?

temperatures, the reaction rate of Cu₂O@PNIPAM core-shell nanoreactors does not follow a simple Arrhenius law with constant activation energy as shown in Figure 5d. Below the LCST, the reaction rate of Cu₂O@PNIPAM core-shell system increased with rising temperature and showed a local maximum at around 25°C. If the temperature was increased close to the LCST, a dramatic decrease of the reaction rate was observed. Then a slight increase of the reaction rate took place with further increasing temperature. This behavior must be assigned to the strong temperature dependence of the overall physicochemical properties of the Cu₂O@PNIPAM core-shell nanoreactors.

The reasons for the temperature induced change of the reaction rate can be qualitatively rationalized by the following arguments. First, from the UV-vis spectra, we found that the core-shell particles can absorb more light at 15°C than at 40°C, thereby signifying that the core-shell particles can produce more active OH radicals at the nanocube at the lower temperature.^{46,47} Secondly, in the collapsed state the gel becomes hydrophobic and likely leads to a local re-partitioning of MO within the PNIPAM-shell: MO is known to situate itself at the interface between water and oil in a surfactant-like style,⁴⁸ meaning that MO could be mostly located in a thin region constituting the hydrogel/solvent interface (see Fig. 6). This view of high adsorption of MO to the hydrogel surface is also supported by the measured zeta potential of the nanoreactors that substantially decreases from a positive +22 mV to a negative -14.3 mV after addition of MO. The re-partitioning and enrichment of MO at the hydrogel/solvent interface, in turn, would lead to a reduced MO concentration adjacent to the nanoparticle. According to our theory²⁴ this depletion of reactants should effectively reduce the rate. Hence, at the lower T, rate enhancement is likely to originate from a combination of increased OH production and a local, MO re-partitioning within the hydrogel shell. However, details of these intricate and very local phenomena are currently difficult to explore and should be interesting for future work.

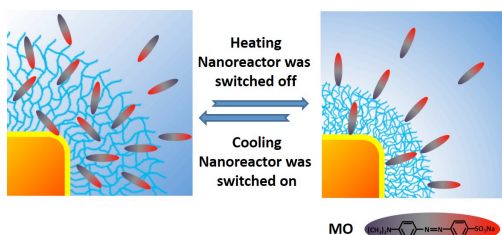


Figure 6. Illustration of the catalytic process. At low temperature the network is fully swollen by water and the hydrophilic dye molecules will be enriched within the network. As a consequence of this, the reaction rate for photocatalysis will be increased. In the shrunken state, the increased solvation free enthalpy of the dye molecules decreases their local concentration, and their diffusion coefficient is also reduced due to a tighter polymer network. Together, these

effects contribute to a strong decrease of the reaction rate for photocatalysis.

Conclusions

In conclusion, we introduce a novel method to synthesize hybrid core-shell microgels consisting of Cu₂O nanocubes as the core and thermosensitive PNIPAM as the shell. The core-shell nanoreactors present much higher colloidal stability than pure Cu₂O nanocubes in water solution. In addition, the PNIPAM shell can effectively protect the Cu₂O nanocubes from oxidation for months. The Cu₂O@PNIPAM core-shell nanoreactors show significant enhancement for the photo decomposition of methyl orange under visible light: the reaction rate of the core-shell nanoreactors is 450 times of that of pure Cu₂O nanocubes at 15°C. Moreover, temperature can be used as a trigger to control the photocatalytic activity of the Cu₂O@PNIPAM core-shell microgels as expected from theory. The present work proves that modification of Cu₂O nanocubes with PNIPAM shell will have a great potential for the applications of Cu₂O nanoparticles, which is essential to understand the effect of PNIPAM shell on properties of metal or metal oxide nanomaterials.

Acknowledgements

S.A.-U. acknowledges the Alexander von Humboldt Foundation (AvH) for funding via an AvH Postdoctoral Research Fellowship. J.D. is grateful for support from the AvH and the ERC (European Research Council) Consolidator Grant with project number 646659 – NANOREACTOR. H. J. gratefully acknowledges the financial support of CSC scholarship. We also thank Dr. Thomas Dittrich (Institute of Heterogeneous Materials, Helmholtz-Center Berlin for materials and energy) for his kind help.

References

- 1 S. Brittman, Y. Yoo, N. P. Dasgupta, S. I. Kim, B. Kim, P. Yang, *Nano Lett.* 2014, **14**, 4665.
- 2 P. Poizot, S. Laruelle, S. Grugeon, L. Dupont, J.-M. Tarascon, *Nature* 2000, **407**, 496.
- 3 S. Deng, V. Tjoa, H. M. Fan, H. R. Tan, D. C. Sayle, M. Olivo, S. Mhaisalkar, J. Wei, C. H. Sow, *J. Am. Chem. Soc.* 2012, **134**, 4905.
- 4 Q. Tian, W. Wu, L. Sun, S. Yang, M. Lei, J. Zhou, Y. Liu, *ACS Appl. Mater. Interfaces* 2014, **6**, 13088.
- 5 Q. Hua, T. Cao, X. K. Gu, J. Lu, Z. Jiang, X. Pan, L. Luo, W. X. Li, W. Huang, *Angew. Chemie - Int. Ed.* 2014, **126**, 4956.
- 6 P. Dai, W. Li, J. Xie, Y. He, J. Thorne, G. McMahon, J. Zhan, D. Wang, *Angew. Chemie - Int. Ed.* 2014, **53**, 13493.
- 7 W. C. Huang, L. M. Lyu, Y. C. Yang, M. H. Huang, *J. Am. Chem. Soc.* 2012, **134**, 1261.
- 8 C. H. Kuo, M. H. Huang, *Nano Today* 2010, **5**, 106.
- 9 A. Paracchino, V. Laporte, K. Sivula, M. Grätzel, E. Thimsen, *Nat. Mater.* 2011, **10**, 456.

- 10 C. G. Morales-Guio, S. D. Tilley, H. Vrubel, M. Grätzel, X. Hu, *Nat. Commun.* 2014, **5**, 3059.
- 11 Z. Zhang, R. Dua, L. Zhang, H. Zhu, H. Zhang, P. Wang, *ACS Nano* 2013, **7**, 1709.
- 12 Z. Zhang, P. Wang, *J. Mater. Chem.* 2012, **22**, 2456.
- 13 H. Yang, Y. Min, Y. Kim, U. Jeong, *Colloids Surfaces A Physicochem. Eng. Asp.* 2013, **420**, 30.
- 14 X. Su, J. Zhao, X. Zhao, Y. Guo, Y. Zhu, Z. Wang, *Nanotechnology* 2008, **19**, 365610.
- 15 J. Dubbert, K. Nothdurft, M. Karg, W. Richtering, *Macromol. Rapid Commun.* 2015, **36**, 159.
- 16 Y. Lu, J.Y. Yuan, F. Polzer, M. Drechsler, J. Preussner, *ACS Nano*, 2010, **4**, 7078.
- 17 M. Kuang, D. Wang, H. M \ddot{o} hwald, *Adv. Funct. Mater.* 2005, **15**, 1611.
- 18 J. Yang, D. Shen, L. Zhou, W. Li, X. Li, C. Yao, R. Wang, A. M. El-Toni, F. Zhang, D. Zhao, *Chem. Mater.* 2013, **25**, 3030.
- 19 S. Wiese, A. C. Spiess, W. Richtering, *Angew. Chemie - Int. Ed.* 2013, **52**, 576.
- 20 Y. Lu, M. Ballauff, *Prog. Polym. Sci.* 2011, **36**, 767.
- 21 Y. Lu, Y. Mei, M. Drechsler, M. Ballauff, *Angew. Chemie - Int. Ed.* 2006, **45**, 813.
- 22 S. Wu, J. Dzubiel, J. Kaiser, M. Drechsler, X. Guo, M. Ballauff, Y. Lu, *Angew. Chemie - Int. Ed.* 2012, **5**, 2229.
- 23 J. Pérez-Juste, I. Pastoriza-Santos, L. M. Liz-Marzán, *J. Mater. Chem. A* 2013, **20**–26.
- 24 S. Angioletti-Uberti, Y. Lu, M. Ballauff, J. Dzubiel, *J. Phys. Chem. C* 2015, **119**, 15723.
- 25 R. Contreras-Cáceres, A. Sánchez-Iglesias, M. Karg, I. Pastoriza-Santos, J. Pérez-Juste, J. Pacifico, T. Hellweg, A. Fernández-Barbero, L. M. Liz-Marzán, *Adv. Mater.* 2008, **20**, 1666.
- 26 R. G. Chaudhuri, S. Paria, *Chem. Rev.* 2012, 2373–2433.
- 27 M. Karg, I. Pastoriza-Santos, L. M. Liz-Marzán, T. Hellweg, *ChemPhysChem*, 2006, **7**, 2298.
- 28 C. H. Kuo, C. H. Chen, M. H. Huang, *Adv. Funct. Mater.* 2007, **17**, 3773.
- 29 K. Henzler, P. Guttman, Y. Lu, F. Polzer, G. Schneider, M. Ballauff, *Nano Lett.* 2013, **13**, 824.
- 30 F. Wang, J. Du, *Chem. Commun.* 2015, **51**, 11198.
- 31 H. Jia, D. Schmitz, A. Ott, A. Pich, Y. Lu, *J. Mater. Chem. A* 2015, **3**, 6187.
- 32 Y. Lu, S. Proch, M. Schrunner, M. Drechsler, R. Kempe, M. Ballauff, *J. Mater. Chem.* 2009, **19**, 3955.
- 33 M. Lin, G. Chen, M. Liang, *Polym. Chem.* 2014, **5**, 234.
- 34 K. Wei, L. Su, G. Chen, M. Jiang, *Polymer*, 2011, **52**, 3647.
- 35 Y. Lu, P. Spyra, Y. Mei, M. Ballauff, A. Pich, *Macromol. Chem. Phys.* 2007, **208**, 254.
- 36 Y. Zhang, B. Deng, T. Zhang, D. Gao, A. Xu, *J. Phys. Chem. C* 2010, **114**, 5073.
- 37 J. Y. Ho, M. H. Huang, *J. Phys. Chem. C* 2009, **113**, 14159.
- 38 H. Zhang, F. Liu, B. Li, J. Xu, X. Zhao, X. Liu, *RSC Adv.* 2014, **4**, 38059.
- 39 C.S. Lao, M.C. Park, Q. Kuang, Y. Deng, A. K. Sood, D.L. Polla, Z.L. Wang, *J. Am. Chem. Soc.* 2007, **129**, 12096.
- 40 Z. Yu, D. Tang, H. Lv, Q. Feng, Q. Zhang, E. Jiang, Q. Wang, *Colloids and Surfaces A: Physicochem. Eng. Aspects*, 2015, **471**, 117.
- 41 T. Hellweg, *Angew. Chemie - Int. Ed.* 2009, **48**, 6777.
- 42 J. Pal, M. Ganguly, C. Mondal, A. Roy, Y. Negishi, T. Pal, *J. Phys. Chem. C* 2013, **117**, 24640.
- 43 A. Tang, Y. Xiao, J. Ouyang, S. Nie, *J. Alloys Compd.* 2008, **457**, 447.
- 44 L. Ghassemzadeh, T.J. Peckham, T. Weissbach, X. Luo, S. Holdcroft, *J. Am. Chem. Soc.* 2013, **135**, 15923.
- 45 S. Stoll, A. Schweiger, *J. Magn. Reson.* 2006, **178**, 42.
- 46 F. Dong, W. Zhao, Z. Wu, S. Guo, *J. Hazard. Mater.* 2009, **162**, 763.
- 47 Q. Xiang, J. Yu, M. Jaroniec, *Phys. Chem. Chem. Phys.*, 2011, **13**, 4853.
- 48 T. FUJIEDA, K. OHTA, N. WAKABAYASHI, S. HIGUCHI, *J. Colloid Interface Sci.* 1997, **185**, 332.

For Table of Contents Use Only

Thermosensitive Cu₂O-PNIPAM core-shell nanoreactors with tunable photocatalytic activity

He Jia,¹ Stefano Angioletti-Uberti,^{1,2} Katja Henzler,³ Andreas Ott,¹ Xianzhong Lin,⁴ Jannik Möser,⁵ Alexander Schnegg,⁵ Joachim Dzubiella,^{1,2} Matthias Ballauff,^{1,2} Yan Lu^{1*}

TOC Figure

Cu₂O-PNIPAM core-shell nanoparticles have been synthesized to protect the Cu₂O nanocubes from oxidation and applied as active “nanoreactors” for the photocatalytic decomposition of methyl orange. A significant enhancement in reaction rate of the core-shell nanoreactors has been observed compared with pure Cu₂O nanocubes. Moreover, the catalytic activity of the embedded Cu₂O nanocubes can be tuned by temperature, which is rationalized by the theory we recently presented.

